Journal of Alloys and Compounds 509 (2011) 9079–9083

Contents lists available at ScienceDirect

Journal of Alloys and Compounds

journal homepage: www.elsevier.com/locate/jallcom

Improvement of the hydrogen storage properties and electrochemical characteristics of $Ti_{0.85}VFe_{0.15}$ alloy by Ce substitution

K. Shashikala[a,*], Asheesh Kumar[a], C.A. Betty[a], Seemita Banerjee[a], P. Sengupta[b], C.G.S. Pillai[a]

[a] Chemistry Division, Bhabha Atomic Research Centre, Mumbai, Maharastra 400 085, India
[b] Materials Science Division, Bhabha Atomic Research Centre, Mumbai, Maharastra 400 085, India

ARTICLE INFO

Article history:
Received 20 April 2011
Received in revised form 3 June 2011
Accepted 8 June 2011
Available online 13 July 2011

Keywords:
Metal hydride
X-ray diffraction
Microstructure
Hydrogen storage
Electrochemical properties

ABSTRACT

The effect of Ce substitution for Ti on the microstructure, hydrogen absorption characteristics and electrochemical properties of $Ti_{0.85-x}Ce_xVFe_{0.15}$ ($x = 0$, 0.02 and 0.05) is studied in detail. In the Ti–V–Fe series, the composition $Ti_{0.85}VFe_{0.15}$ which crystallizes in single phase BCC structure shows the highest hydrogen storage capacity of 3.7 wt%. In the present study, the effect of Ce addition (2 and 5 at%) on the hydrogen absorption properties of $Ti_{0.85}VFe_{0.15}$ has been investigated by X-ray diffraction, electron probe microanalysis (EPMA) and pressure–composition isotherm studies. The hydrogen absorption capacity is found to be higher for the Ce substituted alloys. The alloys $Ti_{0.85}VFe_{0.15}$, $Ti_{0.83}Ce_{0.02}VFe_{0.15}$ and $Ti_{0.80}Ce_{0.05}VFe_{0.15}$ show maximum hydrogen storage capacities of 3.7, 4.02 and 3.92 wt%, respectively. Kinetic studies show that the hydrogen absorption is quite fast for all the three alloys and they reach near saturation value in about 120 s. Electrochemical studies of the Ce (2 at%) substituted alloy, $Ti_{0.83}Ce_{0.02}VFe_{0.15}$ show higher electrocatalytic activity for the hydrogen electrode reactions as compared to Ce-free parent compound, $Ti_{0.85}VFe_{0.15}$.

1. Introduction

Hydrogen storage, in the recent years, has attracted many new and novel materials such as carbon nanotubes, carbon nanofibers, porous metal–organic frameworks, and alantes [1–4]. However, alloys and intermetallic based hydrides continue to be the most sought after materials for practical applications [5]. The alloys can be tuned to improve the hydrogen storage capacity, reversibility, desorption capacity and desorption temperature. Conventional alloys of AB_2 and AB_5 type exhibit low gravimetric density in the range of 1.2–1.4 wt% of hydrogen. The new series of Ti–V and Ti–Cr–V based body centered cubic (BCC) alloys are being explored extensively due to their high hydrogen absorption capacity of ~3 wt% which is almost twice as that of conventional alloys [6–10]. Due to the higher gravimetric storage capacity, these alloys score over the conventional AB_5 alloys used in Ni–MH batteries. The influence of various substitutional elements on the structural, electrochemical and hydrogen storage properties of Ti–V based BCC alloys have been reported by several researchers [11–15].

Recently, we studied the hydrogen absorption properties of a series of $Ti_{1-x}VFe_x$ ($x = 0$, 0.05, 0.75, 0.1 and 0.2) alloys which are known as good tritium storage materials [16]. In this series, $Ti_{0.85}VFe_{0.15}$ which forms in single phase BCC structure is found to have the highest hydrogen storage capacity of ~3.7 wt%. All other compositions in the Ti–V–Fe series consist of BCC main phase and a secondary Laves phase and hence, a lower hydrogen storage capacity [16]. The BCC alloys containing secondary Laves phase are found to have a relatively lower hydrogen absorption capacity. In this study, we attempted to improve the hydrogen absorption characteristics of the BCC $Ti_{0.85}VFe_{0.15}$ alloy by substituting a small amount of Ce (2 and 5 at%) for Ti. Since rare earths have strong affinity towards oxygen, they preferentially react with oxygen, thereby improving the homogeneity of the BCC phase [17–21]. The alloys $Ti_{0.85-x}Ce_xVFe_{0.15}$ ($x = 0$ and 0.02 and 0.05) have been characterized by pressure–composition isotherms studies. The microstructures of the alloys have been characterized by electron probe microanalysis (EPMA) technique. Further, the electrochemical performance of Ce-free and Ce-substituted alloys has been studied.

2. Experimental

The alloys $Ti_{0.85-x}Ce_xVFe_{0.15}$ ($x = 0$, 0.02 and 0.05) were prepared by arc melting high purity elements (>99.9%) under argon atmosphere. The buttons were turned over and remelted 4–5 times to ensure homogeneity. Phase purity of the alloys was checked by X-ray diffraction (XRD) technique using Cu Kα radiation.

X-ray microanalyses of the representative alloys were done using Electron Probe Micro-Analyser (EPMA, CAMECA SX-100 model). For analysis, the alloys were mounted in resin, ground with different grades of emery paper and polished on lapping wheel with diamond paste of 0.25 μm grain size. An acceleration voltage of 20 kV and stabilized beam current of 4 nA and 20 nA were used for 'back scattered electron (BSE)' and quantitative/qualitative analysis, respectively. The beam size

* Corresponding author. Tel.: +91 022 25595093.
E-mail addresses: shashik@barc.gov.in, ksbns@yahoo.com (K. Shashikala).

0925-8388/$ – see front matter © 2011 Elsevier B.V. All rights reserved.
doi:10.1016/j.jallcom.2011.06.034

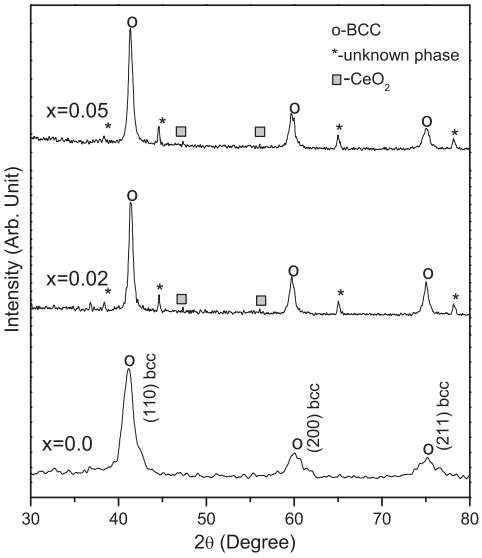

Fig. 1. X-ray diffraction patterns of $Ti_{0.85-x}Ce_xVFe_{0.15}$ alloys with $x = 0$, 0.02 and 0.05.

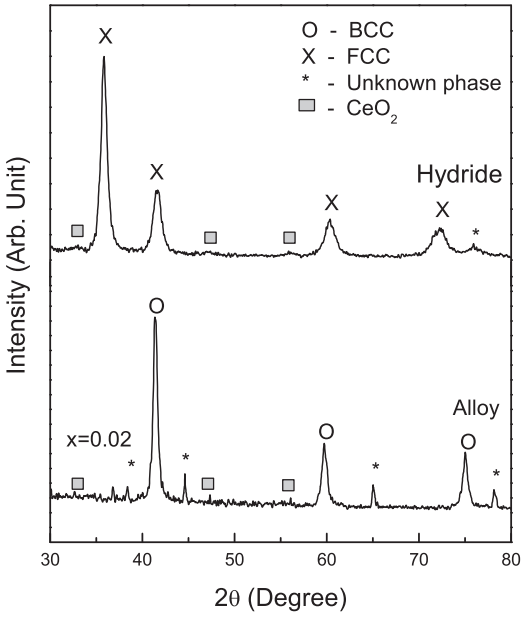

Fig. 2. X-ray diffraction patterns of 2 at% Ce substituted alloy $Ti_{0.83}Ce_{0.02}VFe_{0.15}$ and its hydride $Ti_{0.83}Ce_{0.02}VFe_{0.15}H_{4.26}$.

was kept at <1 μm to reduce the convolution effect so as to arrive at good compositional estimates. Raw intensity data were corrected for atomic numbers, absorption and fluorescence using the PAP (Pouchou and Pichoir) procedure [22].

The hydrogen absorption and desorption characteristics were studied using a Sievert's type set up described in our earlier studies [16,23]. The alloys were activated by heating under a vacuum of 10^{-6} mbar for 2 h at 673 K followed by hydrogen absorption at room temperature. The pressure composition isotherms (P–C) were studied in the pressure range of 0.02–20 atm at 298 K. The kinetic study was done at room temperature and a hydrogen pressure of 20 atm after one absorption–desorption cycle.

Electrochemical measurements were carried out using potentiostat/galvanostat (PGSTAT20, Echochemie, The Netherlands) attached with frequency response analyzer (FRA). The alloy button cut into plate shape was used as working electrode, Ag/AgCl as the reference electrode and platinum wire mesh as the counter electrode. 6 M KOH solution was used as electrolyte. Impedance measurements were carried out using a sinusoidal *ac* excitation signal with peak to peak amplitude of 10 mV and frequency in the range 0.1 Hz to 100 kHz.

3. Results and discussion

3.1. Structural characterisation

Fig. 1 shows the XRD patterns of $Ti_{0.85-x}Ce_xVFe_{0.15}$ ($x = 0$, 0.02 and 0.05) alloys. The XRD pattern indicates that $Ti_{0.85}VFe_{0.15}$ alloy crystallizes in BCC structure with a lattice parameter of 3.086 Å. It is observed from the XRD patterns that Ce substitution for Ti results in a small amount of CeO_2 phase along with the main BCC phase. This observation is in agreement with the earlier works [17–21], wherein a small amount of Ce substitution in $V_{55}Ti_{22.5}Cr_{16.1}Fe_{6.4}$ is reported to result in a secondary CeO_2 phase formation. Since most of the Ce is getting converted into CeO_2, the change in lattice parameter is very small. For example, the lattice parameter changes from 3.086 Å for the Ce-free alloy to 3.095 Å for the 2 at% Ce substituted alloy to 3.097 Å for the 5 at% Ce substituted alloy. We also find peaks due to an additional phase in the Ce substituted alloys, although the exact composition is not known. This phase is not matching with any of the reported phases such as Ti_2FeO_x, $CeTiO_x$ or Ce–Ti alloys. Yan et al. [17] made similar observations in Ce substituted $V_{55}Ti_{22.5}Cr_{16.1}Fe_{6.4}$ wherein these peaks are attributed to unknown phase. Since the composition of our parent alloy $Ti_{0.85}VFe_{0.15}$ is different from the alloy $V_{55}Ti_{22.5}Cr_{16.1}Fe_{6.4}$ studied by Yan et al. [17], the intensity of the X-ray peaks corresponding to unknown phase is at variance.

Fig. 2 shows the XRD patterns of the representative alloy $Ti_{0.83}Ce_{0.02}VFe_{0.15}$ and its hydride, $Ti_{0.83}Ce_{0.02}VFe_{0.15}H_{4.26}$, respectively. The structure changes from BCC to FCC on hydrogenation [16]. The unknown phase does absorb hydrogen. However, the peaks corresponding to the unknown phase are not prominent in the XRD pattern of the hydride except the one at higher angle, 76.25°. This may be due to the partial overlapping of some of the peaks of the hydride of the unknown phase (shifted to the lower 2-theta value upon hydrogen absorption) with the peaks of the main FCC hydride phase. The XRD pattern of the hydride $Ti_{0.83}Ce_{0.02}VFe_{0.15}H_{4.26}$ could be indexed on the basis of FCC structure with lattice parameter 4.350 Å. Similarly, the hydrides $Ti_{0.85}VFe_{0.15}H_{3.83}$ and $Ti_{0.80}Ce_{0.05}VFe_{0.15}H_{4.27}$ are found to have FCC structure with lattice constants 4.292 and 4.350 Å, respectively.

3.2. Microchemical analysis by EPMA

Detailed microchemical analyses of the alloys have been carried out using EPMA technique. The $Ti_{0.85}VFe_{0.15}$ alloy shows a single phase microstructure (Fig. 3(a)) whereas Ce-substituted $Ti_{0.83}Ce_{0.02}VFe_{0.15}$ and $Ti_{0.80}Ce_{0.05}VFe_{0.15}$ alloys exhibit three phase microstructure. Representative back scattered electron image for $Ti_{0.83}Ce_{0.02}VFe_{0.15}$ alloy is shown in Fig. 3(b). It is apparent from the image that there are (i) large bright (roughly 10–15 micron size) and (ii) small bright (roughly 2–5 micron size) phases distributed within single phase matrix. It is noted that the large bright phases have a tendency to cluster at the triple point junctions and grain boundaries whereas small bright phases are more random in nature. Wave-length dispersed X-ray line spectra obtained from each of these different phases indicate that the large bright phase is essentially constituted of Ce and O whereas small bright phase contains significant amount of Ce together with Ti and V. This becomes apparent from the Ce La, Ti Ka and V Ka X-ray line profiles (Fig. 4(a)–(c)). A comparative study of EPMA results with those obtained from XRD analysis show good correlation. Additionally, EPMA data identifies the third unidentified phase of XRD spectra as the one having significant amount of Ce, Ti and V. This may be the same in case of Yan et al. [17] and Wu et al. [18].

3.3. Hydrogen absorption characteristics

The alloys $Ti_{0.95}VFe_{0.15}$, $Ti_{0.83}Ce_{0.02}VFe_{0.15}$ and $Ti_{0.80}Ce_{0.05}VFe_{0.15}$ are found to have maximum hydrogen absorp-

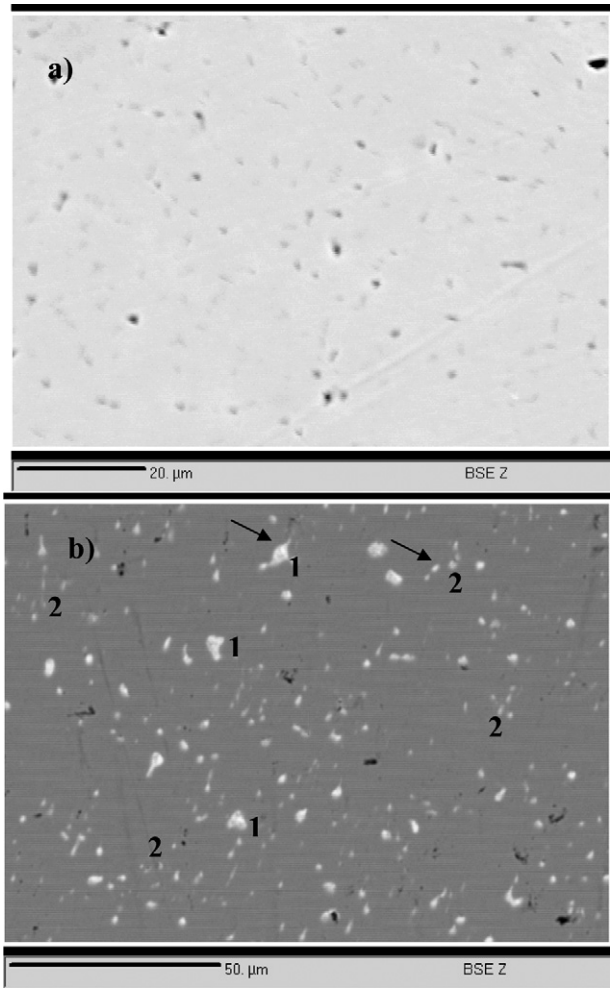

Fig. 3. Electron micrographs of (a) $Ti_{0.85}VFe_{0.15}$ and (b) $Ti_{0.83}Ce_{0.02}VFe_{0.15}$, respectively. Back scattered electron image is showing occurrence of large and small Ce precipitates within the matrix of $Ti_{0.83}Ce_{0.02}VFe_{0.15}$ alloy. Note that the *bright big* areas (marked as 1) are mostly occurring at the triple point junction (marked by black arrows) and *less bright small* areas (marked as 2) are defining the grain boundaries.

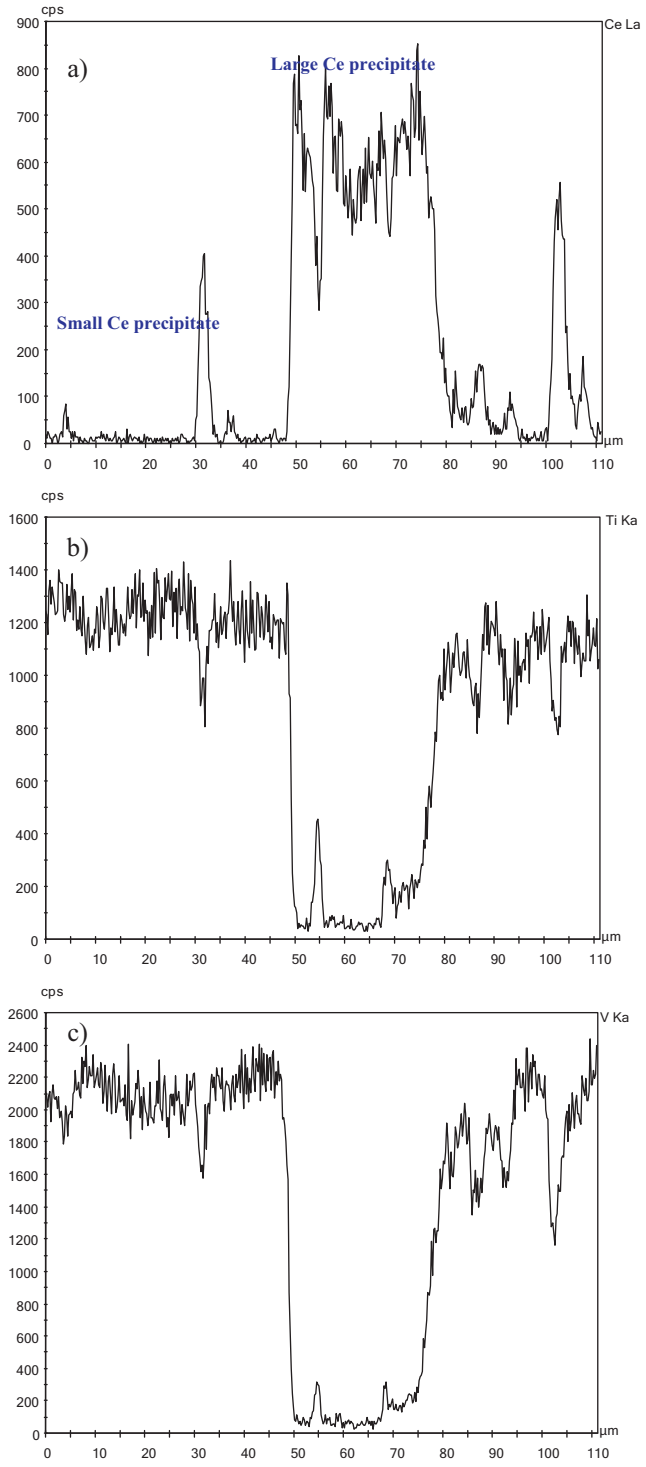

Fig. 4. (a) Ce La, (b) Ti Ka and (c) V Ka X-ray line scans showing compositional variations among different phases of $Ti_{0.83}Ce_{0.02}VFe_{0.15}$ alloy.

tion capacities of 3.7 wt% (H/M = 3.83), 4.02 (H/M = 4.26) and 3.92 wt% (H/M = 4.27), respectively. The hydrogen storage capacities of $Ti_{0.85-x}Ce_xVFe_{0.15}$ alloys as a function of Ce content, *x*, are given in Table 1. The activation of Ce containing alloys is found to be easier as compared to Ce-free alloy. This could be due to the fact that the Ce-containing alloys have a secondary phase with crack formation at the surface so that hydrogen can easily diffuse through the cracks. The rate of hydrogen absorption for all the alloys as a function of time after one absorption–desorption cycle is shown in Fig. 5. It may be noted that the hydrogen absorption rate is quite fast and the hydrides reach near saturation value in about 120 s. Kinetic studies show that the hydrogen absorption is quite fast for all the three alloys.

Fig. 6 shows the pressure–composition isotherms of $Ti_{0.85-x}Ce_xVFe_{0.15}$ ($x = 0.0$, 0.02 and 0.05) alloys at room temperature. For all compositions, the plateau region is found to be <0.02 atm, which is the lowest detection limit of our set up. In general, V based BCC alloys form monohydride and dihydride phases, exhibiting two plateau region in the P–C isotherms [7,8,24]. The plateau corresponding to monohydride exists in the region of low pressure of the order of 10^{-2} mbar, at room temperature. The two plateau region was not observed in the pressure range of this study, as resolving the two plateau region needs pressure measurements in the low pressure region [7,8,24]. As can be seen from the pressure–composition isotherm study, the length of the plateau region increases for the Ce substituted alloys as compared to that of Ce-free alloy, $Ti_{0.95}VFe_{0.15}$. The hydrogen storage capacity of $Ti_{0.85-x}Ce_xVFe_{0.15}$ increases with the increase in Ce content up to $x = 0.02$. Further increase in the Ce content to $x = 0.05$, reduces the hydrogen storage capacity of the alloy marginally.

As seen from EPMA studies, the formation of CeO_2 phase in the BCC phase plays a crucial role in improving the hydrogen storage capacity of Ce substituted alloys. Due to the strong affinity of Ce to

Table 1
Lattice parameters before and after hydrogenation and the maximum storage capacities of the alloys.

Alloy	Lattice parameter of BCC phase (Å)	Hydride composition	Lattice parameter of FCC phase (Å)	Capacity (wt%)
$Ti_{0.85}VFe_{0.15}$	3.086	$Ti_{0.85}VFe_{0.15}H_{3.83}$	4.292	3.7
$Ti_{0.83}Ce_{0.02}VFe_{0.15}$	3.095	$Ti_{0.83}Ce_{0.02}VFe_{0.15}H_{4.26}$	4.350	4.02
$Ti_{0.80}Ce_{0.05}VFe_{0.15}$	3.097	$Ti_{0.80}Ce_{0.05}VFe_{0.15}H_{4.27}$	4.350	3.92

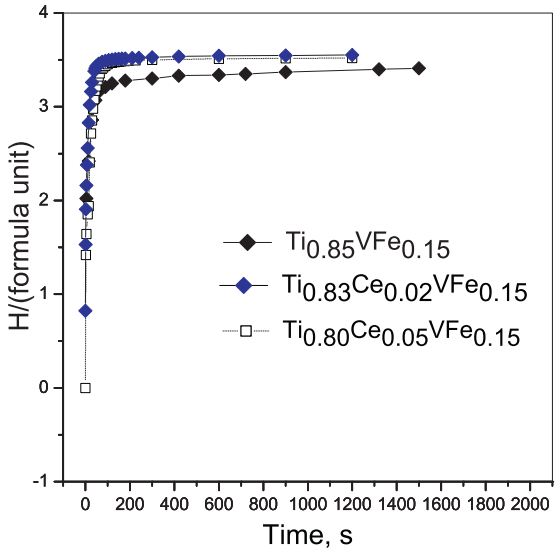

Fig. 5. Kinetic study on $Ti_{0.85}VFe_{0.15}$, $Ti_{0.83}Ce_{0.02}VFe_{0.15}$ and $Ti_{0.80}Ce_{0.05}VFe_{0.15}$ alloys.

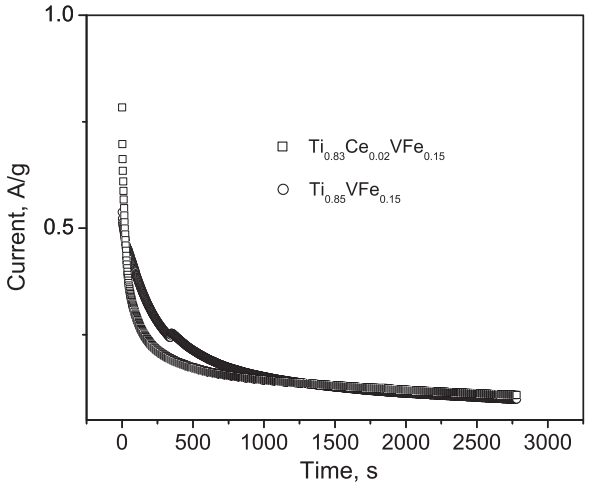

Fig. 7. Current vs. time characteristics of $Ti_{0.85}VFe_{0.15}$ and $Ti_{0.83}Ce_{0.02}VFe_{0.15}$ alloys.

oxygen, Ce preferentially reacts with trace oxygen during melting, thereby, reducing the reaction of Ti with oxygen. This is likely to lead to improved homogeneity of the BCC phase with higher Ti content as mentioned in Refs. [17–21].

3.4. Electrochemical characterization

Electrochemical characterization of the two representative alloys $Ti_{0.85}VFe_{0.15}$ and $Ti_{0.83}Ce_{0.02}VFe_{0.15}$ are presented in this section. From the polarization measurements carried out at small over-potentials (−6 to +4 mV vs. reference electrode) at a scan rate of 1.5 mV s^{-1} for $Ti_{0.85}VFe_{0.15}$ and $Ti_{0.83}Ce_{0.02}VFe_{0.15}$ alloys, the estimated polarization resistance values are 264 and 253 mΩ, respectively. Corresponding exchange current densities calculated are 98 and 108.52 mA g^{-1}. The increased exchange current density of Ce doped alloy indicates improved electrocatalytic activity for the hydrogen electrode reactions. The exchange current density is dependent both on the construction of MH electrode plate and the additives in the electrode plate. An increase in the exchange current density for a battery electrode leads to an increase in the high-rate discharge capability [25].

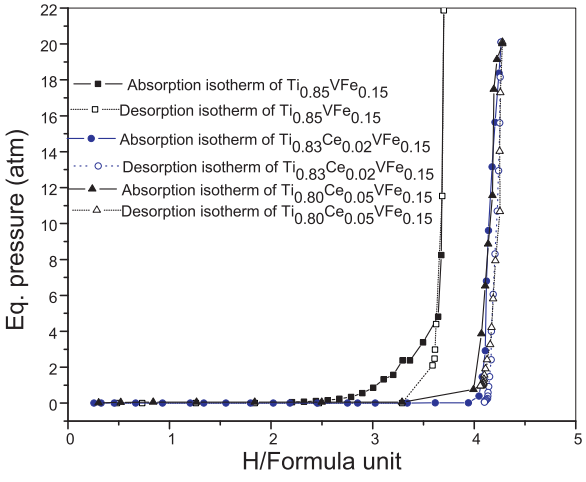

Fig. 6. Pressure–composition isotherms of $Ti_{0.85-x}Ce_xVFe_{0.15}$ (x = 0, 0.02 and 0.05) alloys at room temperature.

Fig. 7 shows the current density vs. time of $Ti_{0.85}VFe_{0.15}$ and $Ti_{0.83}Ce_{0.02}VFe_{0.15}$ alloys (un-charged) measured in KOH electrolyte at a DC voltage of 0.25 V. The initial current density obtained is 538 and 783 mA g^{-1} for $Ti_{0.85}VFe_{0.15}$ and $Ti_{0.83}Ce_{0.02}VFe_{0.15}$ alloys studied with a broad and stable plateau region of ~175–100 mA g^{-1} for both the alloys. It may be noted that the Ce-containing alloy has higher initial current density as compared to that of Ce-free alloy.

Fig. 8 shows the impedance spectra of $Ti_{0.95}VFe_{0.15}$ and $Ti_{0.83}Ce_{0.02}VFe_{0.15}$ (un-charged). The impedance spectra were recorded for $Ti_{0.95}VFe_{0.15}$ and $Ti_{0.83}Ce_{0.02}VFe_{0.15}$ in the frequency range of 0.1 Hz to 100 kHz. Impedance data fitted using a complex non linear least square program shows that contributions for electrode reactions are both from the charge transfer resistance and the diffusion resistance (W). ($R_2 \parallel Q_1$) represents the charge transfer resistance at the electrode/electrolyte interface. R_1 accounts for the contact resistance. The equivalent circuit used for fitting the data is shown in the inset of Fig. 8. Both the samples studied required an inductance element (L_1) for an optimized fit. Diffusion resistance was higher for $Ti_{0.83}Ce_{0.02}VFe_{0.15}$ compared to that of $Ti_{0.95}VFe_{0.15}$.

The anodic oxidation peaks of hydrogen in the cyclic voltammograms were observed at −0.59 V and −0.55 V vs. Ag/AgCl reference electrode respectively, for $Ti_{0.83}Ce_{0.02}VFe_{0.15}$ and $Ti_{0.95}VFe_{0.15}$. The shift of anodic peak potential results from the change of hydrogen diffusivity [26]. The diffusion resistance values of the fitted impedance data also agree with the negative anodic peak shift of the Ce doped sample.

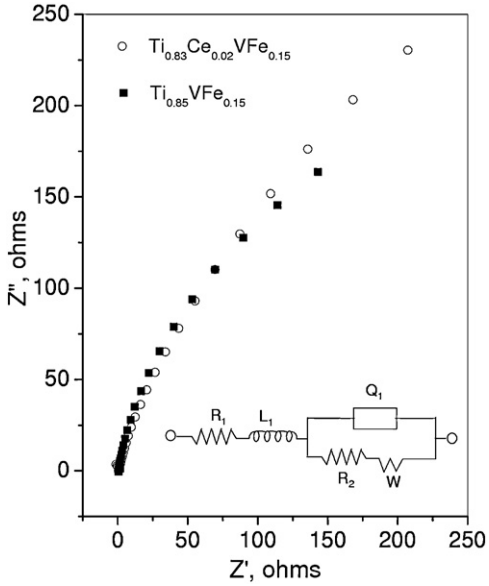

Fig. 8. Measured impedance data plots of $Ti_{0.85}VFe_{0.15}$ and $Ti_{0.83}Ce_{0.02}VFe_{0.15}$ alloys. Inset shows the equivalent circuit used for fitting the data. R_1 is the contact resistance, L_1 is the inductance, $R_2 \parallel Q_1$ represents the charge transfer resistance at the electrode electrolyte interface.

4. Conclusions

In this work, the effect of Ce substitution on the microstructure, hydrogen absorption properties, peak current of hydrogen absorption and electrochemical behaviour of $Ti_{0.85}VFe_{0.15}$ system has been investigated. Substitution of Ce (2 and 5 at%) for Ti is found to improve the hydrogen absorption capacity of $Ti_{0.85}VFe_{0.15}$ alloy. The maximum storage capacity of $Ti_{0.85}VFe_{0.15}$, $Ti_{0.83}Ce_{0.02}VFe_{0.15}$ and $Ti_{0.80}Ce_{0.05}VFe_{0.15}$ alloys are found to be 3.7, 4.02 and 3.92 wt%, respectively. The plateau pressure is found to be <0.02 atm for all compositions. The ease of activation of Ti–V–Fe system is found to improve by Ce substitution. EPMA studies showed the presence of CeO_2 phase in Ce-substituted alloys along with a third phase. Kinetic studies showed that hydrogen absorption is fast for all the three compositions and they reach near saturation in about 120 s. Electrochemical studies showed increased exchange current density for Ce (2 at%) doped alloy indicating improved electrocatalytic activity for the hydrogen electrode reactions.

References

[1] A. Zuttel, P. Sudan, Ph. Mauron, T. Kiyobayashi, Ch. Emmenegger, L. Schlapbach, Int. J. Hydrogen Energy 27 (2002) 203–204.
[2] L. Zaluski, A. Zaluska, J.O. Ström-Olsen, J. Alloys Compd. 253–254 (1997) 70–79.
[3] J.L.C. Rowsell, E.C. Spencer, J. Eckert, J.A.K. Howard, O.M. Yaghi, Science 309 (5739) (2005) 1350–1354.
[4] F. Schüth, B. Bogdanovíc, M. Felderhoff, Chem. Commun. 10 (2004) 2249–2258.
[5] B. Sakintuna, F. Lamari-Darkrim, M. Hirscher, Int. J. Hydrogen Energy 32 (2007) 1121–1140.
[6] K. Nomura, E. Akiba, J. Alloys Compd. 231 (1995) 513–517.
[7] E. Akiba, H. Iba, Intermetallics 6 (1998) 461–470.
[8] T. Kuriiwa, T. Tamura, T. Amemiya, T. Fuda, A. Kamegawa, H. Takamura, M. Okada, J. Alloys Compd. 293–295 (1999) 433–436.
[9] H. Iba, E. Akiba, J. Alloys Compd. 231 (1995) 508–512.
[10] X.B. Yu, Z. Wu, B.J. Xia, N.X. Xu, J. Alloys Compd. 372 (2004) 272–277.
[11] H.G. Pan, R. Li, M.X. Gao, Y.F. Liu, Y.Q. Lei, Q.D. Wang, Int. J. Hydrogen Energy 31 (2006) 1188–1195.
[12] J-.H. Yoo, G. Shim, S.-W. Cho, C.-N. Park, Int. J. Hydrogen Energy 32 (2007) 2977–2981.
[13] S.-J. Qiu, H.-L. Chu, Y. Zhang, L.-X. Sun, F. Xu, Z. Cao, Int. J. Hydrogen Energy 33 (2008) 7471–7478.
[14] M. Tsukahara, K. Takahashi, T. Mishima, A. Isomura, T. Sakai, J. Alloys Compd. 253–254 (1997) 583–586.
[15] H. Miao, M. Gao, Y. Liu, D. Zhu, H. Pan, J. Power Sources 184 (2008) 627–632.
[16] S. Basak, K. Shashikala, P. Sengupta, S.K. Kulshreshtha, Int. J. Hydrogen Energy 32 (2007) 4973–4977.
[17] Y. Yan, Y. Chen, H. Liang, X. Zhou, C. Wu, M. Tao, J. Alloys Compd. 429 (2007) 301–305.
[18] C.L. Wu, Y.G. Yan, Y.G. Chen, M.D. Tao, X. Zheg, Int. J. Hydrogen Energy 33 (2008) 93–97.
[19] X.P. Liu, F. Cuevas, L.J. Jiang, M. Latroche, Z.N. Li, S.M. Wang, J. Alloys Compd. 476 (2009) 403–407.
[20] M.I. Jing, X.P. Liu, L.I. Yan, L. Jiang, L.I. Zhinian, Z. Huang, S.M. Wang, J. Rare Earth 27 (2009) 154–158.
[21] X.P. Liu, L. Jiang, Z. Li, Z. Huang, S. Wang, J. Alloys Compd. 471 (2009) L336.
[22] J.L. Pouchou, F. Pichoir, in: K.F.J. Heinrich, D.E. Newbury (Eds.), Electron Probe Quantitation, Plenum Press, New York, 1991, pp. 31–75.
[23] K. Shashikala, S. Banerjee, Asheesh Kumar, M.R. Pai, C.G.S. Pillai, Int. J. Hydrogen Energy 34 (2009) 6684–6689.
[24] Z. Hang, L. Chen, X. Xiao, S. Li, C. Chen, Y. Lei, Q. Wang, J. Alloys Compd. 493 (2010) 396–400.
[25] M. Geng, J. Han, F. Feng, D.O. Northwood, Int. J. Hydrogen Energy 25 (2000) 203–210.
[26] Y. Wang, X. Wang, Dalton Trans. 40 (2008) 5495–5500.